PHYSICAL REVIEW E **86**, 025302(R) (2012)

Pressure-driven flow through a single nanopore

A. E. Velasco, S. G. Friedman, M. Pevarnik, Z. S. Siwy, and P. Taborek
Department of Physics and Astronomy, University of California, Irvine, California 92697, USA
(Received 17 May 2012; published 22 August 2012)

We have measured the flow of gas through single ion track pores in a polymer film using a mass spectroscopy technique. The pores are 12 μm long with diameters in the range of 50–1000 nm, and the flow was driven by pressure drops in the range 0–30 atm. When the mean free path is large compared to the pore diameter (large Knudsen number Kn), the flow rate is proportional to the pressure drop and the pore radius R cubed, and is consistent with a model of diffusive scattering at the pore walls. For Kn $\leqslant$ 0.1, the hydrodynamic conductance increases, as predicted by standard kinetic theory models, and finally approaches the conventional Poiseuille value with zero slip length.

DOI: 10.1103/PhysRevE.86.025302 PACS number(s): 47.61.−k, 47.45.Dt

Transport of fluids through nanochannels occurs in many biological systems and is an important feature of all nanofluidic sensors and reactors. Although there are many computer simulation studies of transport through individual nanochannels [1–3], experimental measurements are challenging because the mass flow rate through a single nanochannel is typically very small. Most investigations of purely pressure-driven flows through nanochannels have therefore utilized parallel arrays containing many channels [4–8] for which the total flow rates are easier to measure. The inevitable polydispersity of the channels and possible interconnections of pores in large arrays make it difficult to identify dissipation mechanisms and to observe transitions between different types of flow behavior. These issues are important for understanding mass transport at the nanoscale, particularly the violation of conventional hydrodynamic boundary conditions which seem to be required to explain anomalously high flow rates of gases and liquids through carbon nanotube arrays [5,8].

There have been only a few previous studies of pressure-driven flow in single channels of nanometer size. Cheng and Giordano investigated flow through slits that were small in one dimension [9]. Recently, Savard *et al.* have used mass spectroscopy to measure flow through a single nanometer-sized hole [10,11] with an aspect ratio (length/diameter) of approximately 0.5. Here we report measurements using a similar mass spectroscopic technique, but with nanopipes with an aspect ratio in the range of 10–200 in which collisions with the walls establish a pressure gradient along the nanopipe and determine the flow. The radii of the nanochannels can be independently determined using ionic conductivity measurements in aqueous KCl solutions on the same pores. By varying the aspect ratio by an order of magnitude and varying the inlet pressure by approximately four orders of magnitude, our data on the flow rate as a function of the geometry and pressure drop provides a stringent test of hydrodynamic models of pressure-driven flow through nanochannels. The results confirm the applicability of diffuse scattering and no-slip boundary conditions for the description of transport through our pores for diameters as small as 50 nm.

The nanochannels were prepared by passing a single heavy ion (Xe, Au, or Pb) through a 12-mm-thick polyethylene terephthalate (PET) membrane and then symmetrically etching the ion track in diluted sodium hydroxide. This procedure is known to result in cylindrically shaped channels [12]. The final nanochannel diameter was determined by using an ion conductivity method [13–16]. Experimental details are described in the Supplemental Material [17].

A PET membrane containing the etched nanochannel is sealed in a stainless-steel fixture using indium o-rings and attached to a vacuum system. The low-pressure side of the membrane is equipped with a turbo pump, a Pirani gauge, a calibrated leak, and a residual gas analyzer (Stanford Research Systems), while the high-pressure side has a connection to a source of gas and conventional capacitance pressure gauges which together can measure pressures in the range 10^{-2}–10^{4} Torr. The residual gas analyzer (RGA) is essentially a mass spectrometer which converts the current corresponding to a given mass into an effective partial pressure. Using the channel electron multiplier, the minimum detectable partial pressure is approximately 5×10^{-14} Torr. The high sensitivity to a single species and relative insensitivity to background outgassing makes the RGA well suited for this measurement.

Although the RGA directly measures the pressure P, our primary interest is in the mass flow rate through the nanochannel Q; they are related by the pumping speed S, with $Q = SP$. The pumping speed is a geometric property of the pumps and tubing in the vacuum system [18], and can be estimated to within a factor of 4, but for precise work, it is necessary to calibrate the detector. This was accomplished by using a calibrated leak which produced a known mass flow rate. For helium, we used a NIST certified calibrated leak which produced 4.45×10^{12} atoms/s, but it was important to pump on the calibrated leak until it reached a steady-state flow rate. The pumping speed for helium for our configuration can be adjusted in the range 10^{18}–10^{16} atoms/(Pa s).

Helium is a good choice for these transport studies because the background signal at mass 4 amu is very low so flow rates as small as 10^{6} atoms/s can be detected. A disadvantage of helium is that it diffuses readily through many materials. We found that the diffusion rate of helium through an unetched 12-μm PET membrane at room temperature was greater than the flow rate through many of our nanochannels. Measurements of the permeation rate of helium through a solid PET membrane as a function of temperature and pressure difference showed that the flux at 150 K was more than two orders of magnitude smaller than at room temperature, and at 100 K, the diffusive

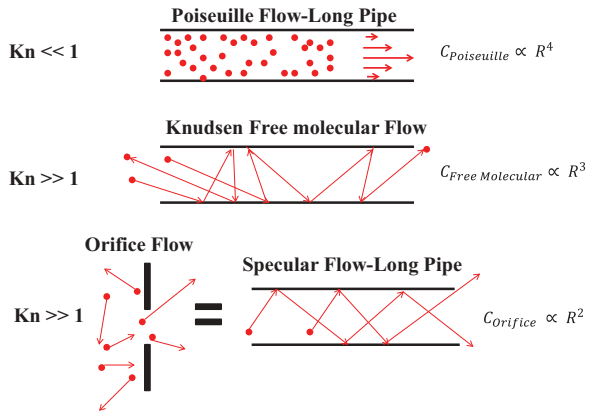

FIG. 1. (Color online) Top: Dense fluid flowing through a pipe in the continuum regime. Particle-particle interactions are important, and the mass flow rate Q and the conductance C are proportional to R^4. Middle: Flow of a rarefied gas in a long pipe with diffusive scattering at the walls. C is proportional to R^3. Bottom: Flow of rarefied gas through an orifice is equal to the number of particles incident on the area of the aperture which scales as R^2. A long pipe with specular reflection at the walls has the same conductance.

flux through our 12-μm membrane was undetectably small even for pressure differences of 20 atm. To eliminate the effects of diffusion, all of our measurements using helium were conducted with the membrane fixture in a bath of liquid nitrogen at 77 K; further details are discussed in the Supplemental Material [17].

The flow rate Q through a flow impedance is proportional to the pressure drop ΔP across it; the proportionality constant C is called the conductance, with $Q = C\Delta P$. The conductance is a function of the geometry of the impedance and the physical properties of the fluid. Detailed models for the conductance exist for several idealized flows illustrated in Fig. 1 which are distinguished by the value of dimensionless parameters including the Knudsen number Kn, which is the ratio of the mean free path in the fluid to the diameter of the channel, and the aspect ratio L/D. There are several definitions of Kn used in the literature. To facilitate comparison to standard models, we have used the definition of Ref. [19] which is based on experimentally determined values of the shear viscosity η:

$$\mathrm{Kn} = \frac{\eta\sqrt{2\pi k_B T}}{2DP\sqrt{m}}, \tag{1}$$

where D is the pore diameter, P is the pressure, and m is the molecular mass. Values of η for helium were taken from Ref. [20]. Alternative definitions of Kn based on an estimate of molecular size neglect interactions and can differ from the definition of Eq. (1) by up to an order of magnitude.

The simplest case to analyze is flow of a rarefied gas ($\mathrm{Kn} \gg 1$) through an orifice ($L/R \simeq 0$) shown in the bottom of Fig. 1. Elementary kinetic theory shows that the particle flux in an ideal gas at pressure P is $P/\sqrt{2\pi m k_B T}$. If the pressure on the low-pressure side of the orifice is zero, the driving pressure drop $\Delta P = P$ and the conductance of the orifice is proportional to the area πR^2. It is interesting to note that the conductance of a long tube is the same as an orifice if particles reflect specularly from its walls. In this case, every particle that enters the tube will leave from the low-pressure side and the conductance is independent of tube length. If the particles reflect diffusely, some particles which enter the tube will diffusively scatter back into the high-pressure reservoir. In the limit of a very long tube, the probability that a particle which has entered the tube emerges from the low-pressure side can be calculated exactly [21]; the result is $\frac{8R}{3L}$.

If $\mathrm{Kn} \gg 1$ the particles do not interact in the tube and the particle trajectories are independent of each other. In the opposite limit of a dense fluid with $\mathrm{Kn} \ll 1$, the particle motions are highly correlated and flow occurs along streamlines. Conventional no-slip boundary conditions imply that the flow velocity along streamlines at the wall is zero. For fluid flow at low velocity, viscous interactions between different streamlines generate a parabolic velocity profile which leads to the Poiseuille formula for the conductance which scales as R^4.

Figure 1 shows that for the simple regimes of either continuum or diffusive flow, the conductance scales as R^n, where $n = 2$, 3, or 4 depending on Kn and the boundary condition. For flows in the intermediate regime where $\mathrm{Kn} \sim 1$, a more sophisticated model is required, and there are two standard approaches that are commonly used. One method invokes a slip length and constructs an interpolation formula which smoothly bridges the two flow regimes [22]. Another method is based on a detailed numerical solution of the Boltzmann equation [19]. Both methods account for the fact that the pressure and therefore Kn vary along the tube, and both models give similar predictions as shown in Fig. 2. Both models asymptotically approach the Knudsen free molecular

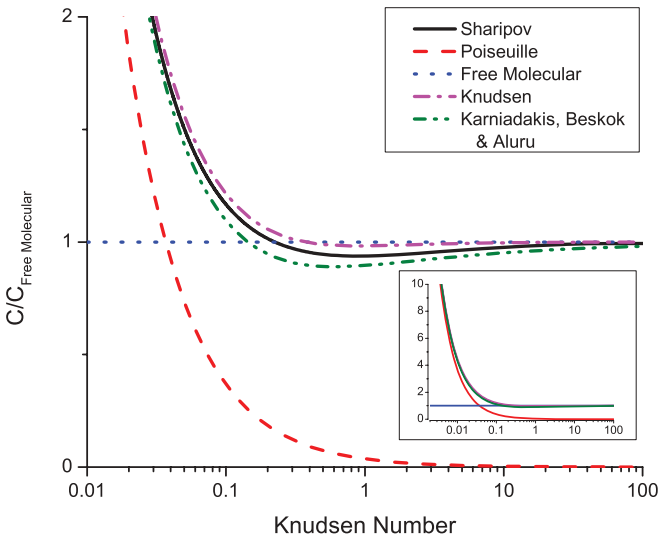

FIG. 2. (Color online) Comparison of various models of the conductance of a long pipe as a function Knudsen number at the inlet. All conductances are normalized by the Knudsen free molecular value $\frac{8\pi}{3L\sqrt{2\pi m k_B T}} R^3$ which is valid at large Kn and is represented by the horizontal blue dotted line. The dashed red curve is the normalized conductance for viscous laminar Poiseuille flow which is physically valid only for $\mathrm{Kn} < 0.01$. The solid black curve is the theory of Ref. [19]. The green dashed-dotted curve is the unified theory described in Ref. [22] and the magenta dashed-dotted curve is the generalized Knudsen theory. The inset contains the same plot on an expanded scale which shows how all of the predictions (including simple Poiseuille flow) merge for $\mathrm{Kn} < 0.01$.

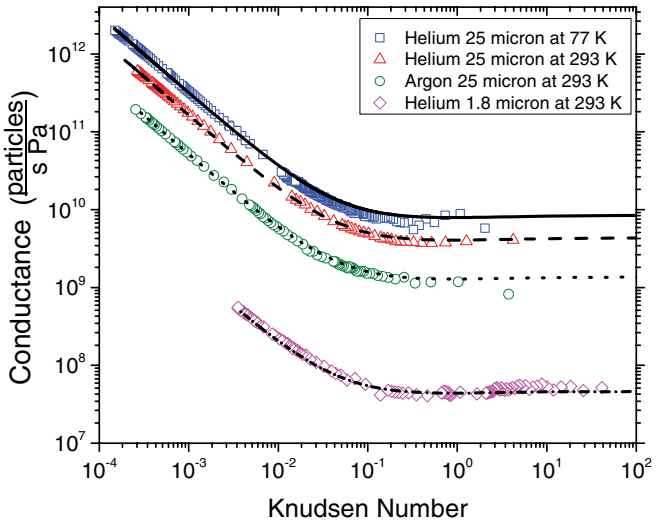

FIG. 3. (Color online) The conductance of a nickel pipe of diameter 25 μm and length 29 cm and a glass capillary 1.8 μm in diameter and 1 cm long as a function of the Knudsen number at the high-pressure end. The low-pressure end is held at $P = 0$. Measurements were done at room temperature and 77 K using helium and argon. Red triangles, blue squares, and green circles are measurements using the nickel tube, while the magenta diamonds are measurements using the glass capillary. The black curves are kinetic theory calculations for each temperature and gas species from Eq. (2). The pressure corresponding to the lowest values of Kn is approximately 10 atm, while the highest values of Kn correspond to pressures near 0.01 Torr.

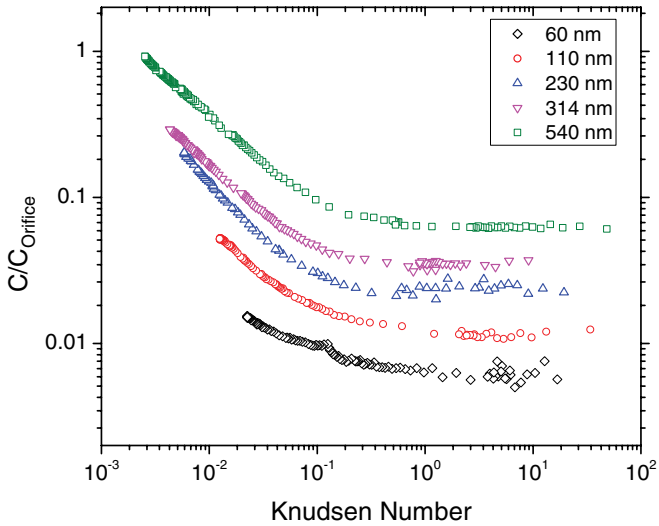

FIG. 4. (Color online) The conductance of pores normalized by the conductance of an orifice of the same diameter as a function of the Knudsen number at the high-pressure end. The fluid is ^{4}He gas at $T = 77$ K. The inside diameter of the pore listed in the legend is the diameter determined from ionic conductivity measurements; the same values were used to compute Kn. The pressure ranges from approximately 31 atm at the low Kn end to 0.01 Torr at the high Kn end.

flow value at large Kn and the Poiseuille value at low Kn; they differ slightly in the transition region Kn $\sim$ 1, where there is a shallow minimum in the conductance. These results have been previously experimentally verified for arrays of tubes with a diameter of 110 μm [23].

As a consistency check on our experimental procedure, we measured the conductance of a nickel tube 25 μm in diameter (Valco Instruments) and 0.29 m long and a glass capillary (Polymicro) 1.8 μm in diameter and 1 cm long using helium and argon at room temperature and at 77 K; the data are shown in Fig. 3. For helium, the relation between helium flow rate and the RGA reading was established by using the calibrated leak as described above. The flow measurements with helium verified the Knudsen formula for large Kn. For argon the flow values in the Poiseuille regime at small Kn were used to calibrate the RGA readings. Viscosity data for argon was taken from Ref. [24]. The kinetic theory predictions for the conductance C are generated by numerically integrating the expression

$$C = \frac{1}{\Delta P L} \int_{P_2}^{P_1} \frac{\pi R^3 \sqrt{m}}{\sqrt{2 k_B T}} G(\delta) dP \qquad (2)$$

from the inlet pressure P_1 to the outlet pressure P_2, which is approximately zero in all of our measurements. $G(\delta)$ is an interpolating function valid for isothermal flow and completely diffuse scattering given in Ref. [25], where $\delta = \sqrt{\pi}/(4\mathrm{Kn})$, which is an implicit function of pressure. The dependence of the conductance on Kn, temperature, and molecular mass is accurately described by the kinetic theory results.

We performed similar flow measurements on several nanochannels in PET membranes with a fixed length (12 μm) but with diameters (as determined by ionic conductivity measurements) ranging from 50 to 1000 nm. The conductance through the nanochannel normalized to the conductance of an orifice in the ballistic limit ($\pi R^2/\sqrt{2\pi m k_B T}$) is shown in Fig. 4 as a function of the Knudsen number at the tube entrance.

The conductance ratio becomes independent of Kn for Kn $>$ 1. To determine the power-law dependence on R in this regime, the average value of the absolute conductance for Kn $>$ 1 as a function of R is shown as a log-log plot in Fig. 5. The solid line is the prediction of Knudsen free molecular theory for the conductance of ^{4}He at $T = 77$ K with no adjustable parameters. For comparison, the dashed line is the conductance of an orifice of radius R which is proportional to R^2. It is clear that the conductance scales as R^3 and that the results are consistent with the Knudsen theory, which is based on the assumption of diffuse reflection at the channel wall for all the channels we investigated. Since this analysis is based on the channel radius inferred from the ionic conductivity, this result also shows that the channel radius determined by ionic conductivity in a liquid and by conductance measurements in a rarefied gas are equivalent.

Since the conductance at large Kn is well described by the diffuse reflection Knudsen free molecular theory, it is useful to normalize the conductance data with respect to the Knudsen conductance, which is shown in Fig. 6. With this normalization, all of the data for the various pores collapse onto a single universal curve.

We have utilized an RGA to make measurements of pressure-driven flow through individual nanometer-scale channels for a wide range of pressure drops and Knudsen numbers

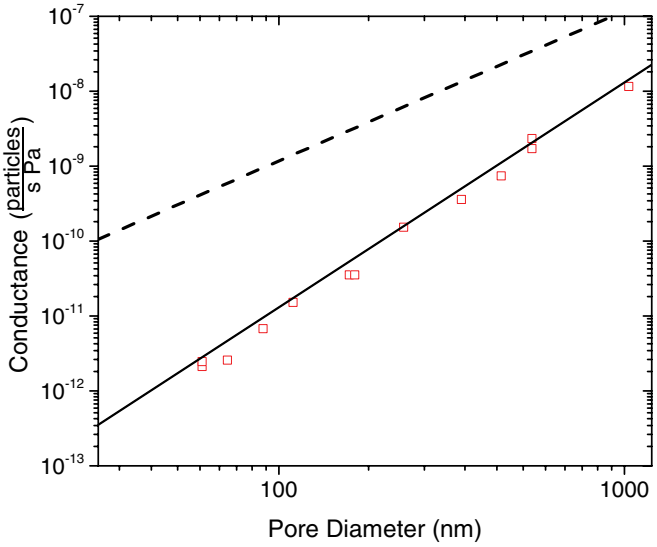

FIG. 5. (Color online) Log-log plot of the conductance of pores in the Kn $>$ 1 regime as a function of nanochannel diameter $D = 2R$. Red squares are data such as those shown in Fig. 4 for pores with a wide range of diameters. The solid line is the Knudsen free molecular theory for a long tube, which scales as R^3; the dashed line is the conductance of an orifice which scales as R^2.

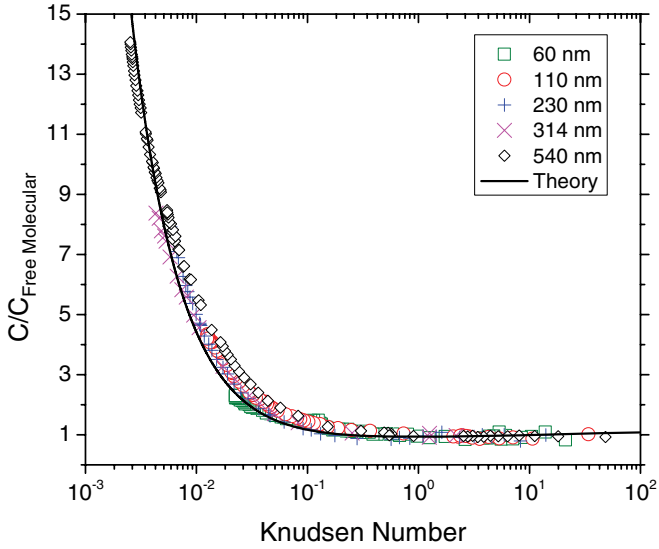

FIG. 6. (Color online) Conductance of nanochannels normalized to the Knudsen free molecular conductance over a wide range of Kn. The pore diameters in the legend were determined from ionic conductivity measurements and were also used to compute Kn. The solid black curve is the theory of Ref. [19], which provides an excellent representation of all of the data over the entire range of Kn.

which includes the transition from free molecular flow to continuum flow. These are measurements on single submicron channels which encompass both flow regimes. The measured conductances have been compared to detailed kinetic theory calculations which become equivalent to the Knudsen formula in the free molecular regime and to the Poiseuille formula for small Kn. Our conductance measurements are in good agreement with these flow models for Kn throughout the range 10^{-3}–10^{2}. Comparison of our flow data to the models requires knowledge of the channel diameter, which we obtained from ionic conductivity measurements. The good agreement we obtain with kinetic theory flow models implies that the channel diameter deduced from ionic conductivity is equivalent to the diameter deduced from conventional flow impedance measurements and provides a self-consistency check for both methods. For Kn $>$ 1, our results are consistent with completely diffuse scattering at the tube wall. Similar results were obtained by Gruener and Huber [7] for arrays of 12-nm pores in silicon at high Kn. By systematically varying the channel radius R, our measurements explicitly show the R^3 dependence of the conductance in this regime. For Kn $<$ 0.01, our results are consistent with conventional hydrodynamics with zero slip at the wall. These results on polymer pores which are rough (the average roughness is typically several percent of the pore radius) [26,27] stand in contrast to results on flow through carbon nanotubes [5,8], which show flow conductances several orders of magnitude larger than the hydrodynamic predictions. These enhanced conductances are presumably due to the extremely smooth walls of nanotubes and the fact that nanotubes are more than an order of magnitude smaller in diameter than the pores investigated here.

This work was supported by the National Science Foundation DMR-0907495 and AFOSR FA9550-12-1-0065. Irradiation with swift heavy ions was performed at the Helmholtzzentrum für Schwerionenforschung, Darmstadt, Germany (GSI).

[1] G. Hummer, J. Rasaiah, and J. Noworyta, Nature (London) **414**, 188 (2001).
[2] J. Goldsmith and C. C. Martens, PhysChemChemPhys **11**, 528 (2009).
[3] Y. Li, J. Xu, and D. Li, Microfluid. Nanofluid. **9**, 1011 (2010).
[4] M. Majumder, N. Chopra, R. Andrews, and B. Hinds, Nature (London) **438**, 44 (2005).
[5] J. K. Holt, H. G. Park, Y. M. Wang, M. Stadermann, A. B. Artyukhin, C. P. Grigoropoulos, A. Noy, and O. Bakajin, Science **312**, 1034 (2006).
[6] M. Whitby and N. Quirke, Nat. Nanotechnol. **12**, 87 (2007).
[7] S. Gruener and P. Huber, Phys. Rev. Lett. **100**, 064502 (2008).
[8] M. Majumder, N. Chopra, and B. J. Hinds, ACS Nano **5**, 3867 (2011).
[9] J. T. Cheng and N. Giordano, Phys. Rev. E **65**, 031206 (2002).
[10] M. Savard, C. Tremblay-Darveau, and G. Gervais, Phys. Rev. Lett. **103**, 104502 (2009).
[11] M. Savard, G. Dauphinais, and G. Gervais, Phys. Rev. Lett. **107**, 254501 (2011).

[12] M. R. Powell, I. Vlassiouk, C. Martens, and Z. S. Siwy, Phys. Rev. Lett. **103**, 248104 (2009).
[13] Z. Siwy, P. Apel, D. Baur, D. D. Dobrev, Y. E. Korchev, R. Neumann, R. Spohr, C. Trautmann, and K.-O. Voss, Surf. Sci. **532–535**, 1061 (2003).
[14] R. B. Schoch, J. Han, and P. Renaud, Rev. Mod. Phys. **80**, 839 (2008).
[15] H. Liu, J. He, J. Tang, H. Liu, P. Pang, D. Cao, P. Krstic, S. Joseph, S. Lindsay, and C. Nuckolls, Science **327**, 64 (2010).
[16] C. Y. Lee, W. Choi, J.-H. Han, and M. S. Strano, Science **329**, 1320 (2010).
[17] See Supplemental Material at http://link.aps.org/supplemental/10.1103/PhysRevE.86.025302 for details regarding the experimental procedure.
[18] J. H. Moore, C. C. Davis, and M. A. Coplan, *Building Scientific Apparatus: A Practical Guide to Design and Construction*, 2nd ed. (Addison-Wesley, London, 1983).
[19] F. M. Sharipov and V. D. Seleznev, J. Vac. Sci. Technol. A **12**, 2933 (1994).
[20] W. Licht and D. Stechert, J. Chem. Phys. **48**, 23 (1944).
[21] P. Clausing, J. Vac. Sci. Technol. A **8**, 636 (1971).
[22] G. Karniadakis, A. Bestok, and N. Aluru, *Microflows and Nanoflows: Fundamentals and Simulation* (Springer, New York, 2005).
[23] L. Marino, Microfluid. Nanofluid. **6**, 109 (2009).
[24] E. W. Lemmon and R. T. Jacobsen, Int. J. Thermophys. **25**, 83 (2004).
[25] F. Sharipov, I. Graur, and C. Day, J. Vac. Sci. Technol. A **28**, 443 (2010).
[26] S. Muller, C. Schotz, O. Picht, W. Sigle, P. Kopold, M. Rauber, I. Alber, R. Neumann, and M. Toimil-Molares, Cryst. Growth Des. **12**, 615 (2012).
[27] M. Pevarnik, K. Healy, M. E. Toimil-Molares, A. Morrison, S. E. Létant, and Z. S. Siwy, ACS Nano (2012).